Air–Ice–Ocean Momentum Exchange. Part I: Energy Transfer between Waves and Ice Floes

W. PERRIE AND Y. HU

Physical and Chemical Sciences, Scotia–Fundy Region, Department of Fisheries and Oceans, Bedford Institute of Oceanography, Dartmouth, Nova Scotia, Canada

(Manuscript received 20 December 1994, in final form 18 October 1995)

ABSTRACT

The energy exchange between ocean surface waves and ice floes in the marginal ice zone (MIZ) involves the scattering and attenuation of wave energy and the excitation of oscillation modes of the ice floes, as open ocean waves propagate into the MIZ. Heave, pitch, and roll modes of oscillation are linked to estimation of wave scattering and attenuation. A model is presented for wave attenuation and compared to measurements from the Marginal Ice Zone Experiments in the Greenland Sea, as reported by Wadhams et al.

1. Introduction

Ice is observed on the Grand Banks of Newfoundland every spring. Ice edge variability involves interactions between ice floes, wind, waves, and currents, which can move the ice edge by as much as 50 km in a single day during high wind and wave situations. Ice edge predictability and the internal ice floe distribution within the Marginal Ice Zone (MIZ) are difficult to forecast on short timescales such as hours or days. As compared to the ice-free situation, nonlinear energy transfer, S_{nl}, due to wave–wave interactions among surface waves, is altered by the distribution of ice floes. Energy input to the wave spectrum S_{in}, due to the wind, the associated planetary boundary layer, as well as dissipation and wave breaking in the wave spectrum, S_{ds}, are also altered from the ice-free situation. As waves are scattered and attenuated by the ice floes, wave energy is transferred to the ice floes, exciting heave, pitch, and roll oscillation modes. Wave energy is also dissipated by the development of wave-induced currents and ice floe drift. In this study, we present a model for the scattering and attenuation of ocean surface waves within the MIZ, hereafter referred to as the *scattering* model. We compare the attenuation predicted by the *scattering* model with model estimates by Liu and Mollo-Christensen (1988).

It was suggested by Masson and LeBlond (1989) that ocean wave spectra within the MIZ should obey the balance equation for wave spectra

$$\frac{\partial E(f,\vartheta)}{\partial t} + \vec{C}_g \cdot \nabla E(f,\vartheta) = (S_{in} + S_{ds})(1 - \mathrm{fi}) + S_{nl} + S_{ice}, \quad (1)$$

where S_{ice} is the change in energy due to wave interactions with ice floes, $\vec{C}_g$ is the group velocity, and fi is the fraction of ocean surface covered by ice. Modern operational wave models perform an integration of Eq. (1), excluding S_{ice} and assuming fi = 0. Thus, the two-dimensional wave spectrum $E(f, \vartheta)$ is determined as a function of frequency f, direction ϑ, and position–time $(\mathbf{x}, t)$ coordinates. Wind input parameterizations, S_{in}, are largely motivated by experimental field work reported in Snyder et al. (1981), modified by numerical experiments by Hasselmann et al. (1988) and others. Nonlinear transfer, S_{nl}, is expressed in terms of an approximation of the original formulations derived by Hasselmann (1962). An example of its use is in the WAM model of Hasselmann et al. (1988). Expressions for dissipation S_{ds} originate from Hasselmann (1974), with some modification to achieve acceptable fetch-growth characteristics, as given by Hasselmann et al. (1988). The manner in which S_{in}, S_{ds}, and S_{nl} balance and combine with one another is discussed by Komen et al. (1984), Phillips (1985), Hasselmann et al. (1988).

Our parameterization of S_{ice} follows Masson and LeBlond (1989) and Isaacson (1982), with some corrections. Thus, we use Green's functions and assume (i) single scattering, (ii) the Foldy–Twersky integral equations (Ishimaru 1978), (iii) ice floes are identical cylinders located at regular hexagonal lattice points within an infinite array, and (iv) the cumulative effect of wave scattering within the MIZ involves linear superposition. Masson and LeBlond (1989) showed that

Corresponding author address: Dr. William Perrie, Bedford Institute of Oceanography, P.O. Box 1006, Dartmouth, NS B2Y 4A2, Canada.

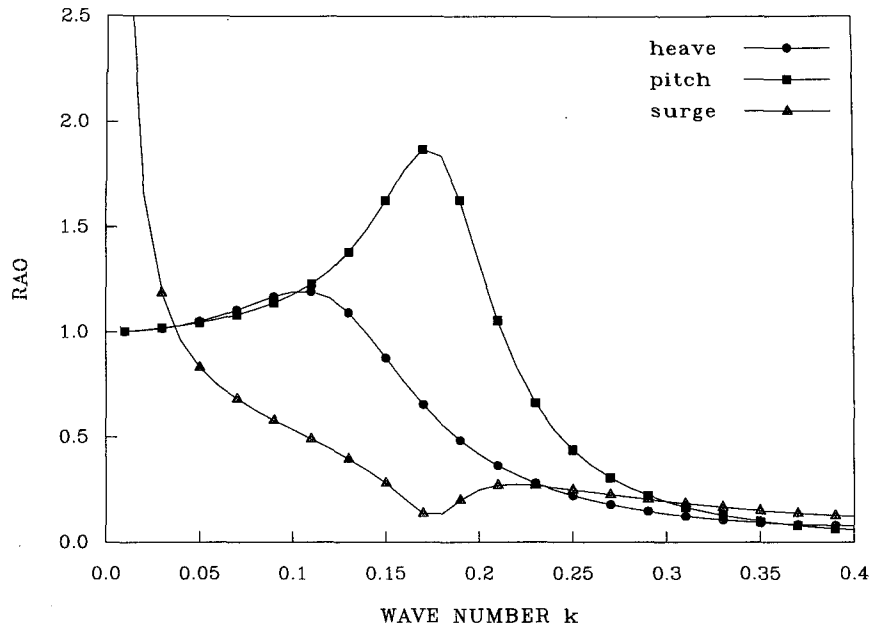

FIG. 1. Heave, pitch and roll RAOs for a cylindrical ice floe of thickness 3 m, radius 10 m, in water 30 m deep using $N = 15$ and $b = 1, 2, 3$ in Eq. (11). We replace $\Sigma_{m=0}^{\infty}$ by $\Sigma_{m=0}^{6}$, in determining the source strength functions, $f_{bl}(s_j)$ in Eqs. (15)–(23).

scattering amplitude and directional properties are dependent on the ratio of the ice floe diameter to wavelength. In addition to ice floe diameter, we take account of floe thickness, ice cover concentration, position within the MIZ, and wave age.

The Liu and Mollo-Christensen (1988) model is essentially a viscous boundary-layer model for wave attenuation. They derive the dispersion relation for waves under pack compression, find the group velocity, calculate the mean compressive stress for buckling failure in the pack, examine the exchange of momentum between waves and the ice pack, and show that pack compression can change the rate of wave packet growth. A problem with this approach is that the expression for wave attenuation ultimately depends on eddy viscosity ν, which can range from 1 to 10^3 cm^2 s^{-1} for the open ocean. For the MIZ, ν depends on the roughness of the underside of the ice cover concentration and is difficult to measure, as suggested by Liu et al. (1991).

Section 2 suggests a parameterization of the ice source term S_{ice} for use in an operational wave model: this allows for scattering of waves by the presence of ice floes. Section 3 presents how scattering depends upon ice floe diameter d, ice floe distribution, and ice thickness. Section 4 presents estimates of the effects of floe diameter and ice cover on wave spectra. Section 5 compares *scattering* model estimates of wave attenuation with observations from the Marginal Ice Zone Experiment (MIZEX) as reported by Wadhams et al. (1986). Throughout this paper, MIZ ice floes are assumed not to drift. Effects of ice drift are given in Part II (Perrie and Hu 1996; manuscript submitted to *J. Phys. Oceanogr.*).

2. Energy transfer between ice and waves

Considerable effort has been devoted to numerical solutions of the energy balance equation (1) for waves in the absence of ice. The resulting progression of wave models include, on one extreme, the empirically tuned operational models. They require a minimum of computational effort and produce reasonable estimates of wave parameters, such as the peak frequency f_p and directional properties of the wave field. On the other extreme are more sophisticated research models that attempt a more detailed description of the dynamics of wave field generation and propagation. An example of such a model is the WAM model of Hasselmann et al. (1988). We use a comparatively simple well-tuned operational model to generate waves for a given wind field because we are concerned with the attenuation and scattering of waves due to the MIZ ice floes. Specifically, we use a second-generation wave model, as described by Resio (1981), Perrie and Toulany (1985) and Perrie et al. (1989).

Waves propagate into the MIZ, or are generated within the MIZ, and experience attenuation and scattering. This is represented by S_{ice} in the balance equation (1), which gives the change in $E(f, \vartheta)$ due to ice floes. Following Isaacson (1982) and Masson and LeBlond (1989), we parameterize S_{ice} assuming a uniform hexagonal lattice of identical, freely floating ice

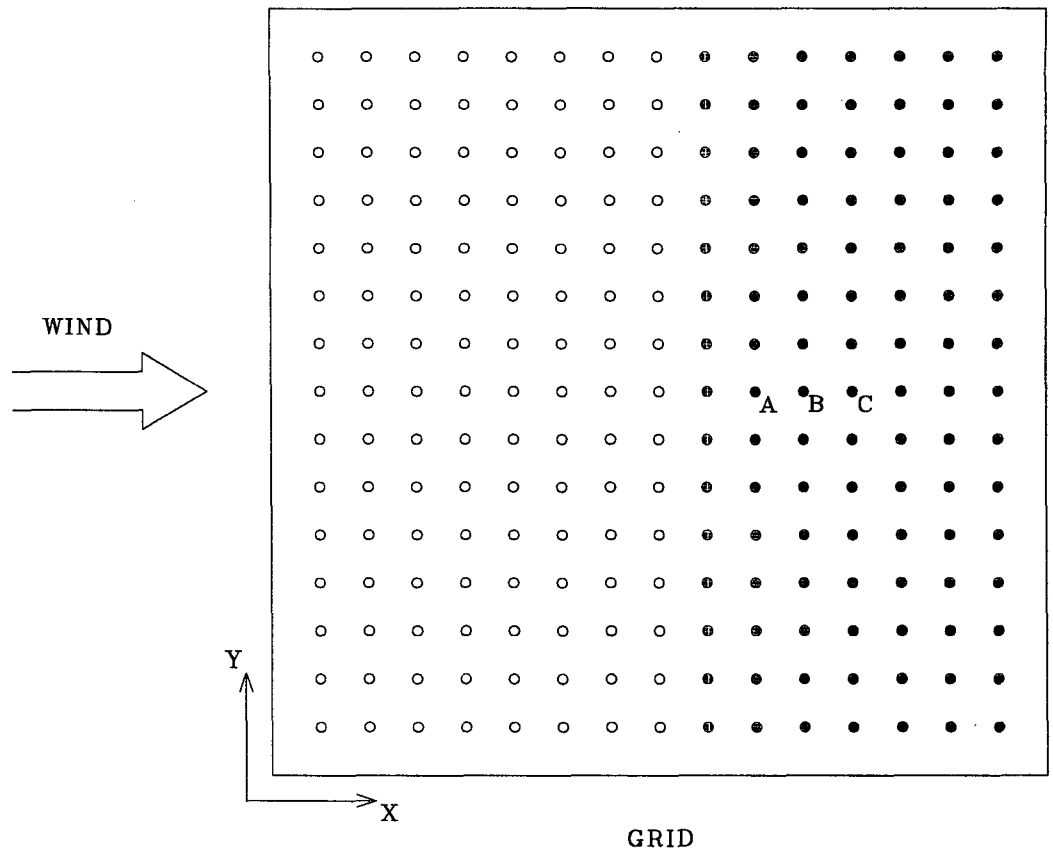

FIG. 2. Grid for the SWAMP square-box ocean of Hasselmann et al. (1985). Wind is in the positive X-axis direction. Ice is indicated by ●. Gridpoint separations in both X and Y directions represent 10 km, uniformly.

floes, within the MIZ. The ice term S_{ice} is expressed in terms of a transformation tensor T^{ij}_{fi}:

$$S(f_i, \vartheta_i)_{\text{ice}} = E(f_i, \vartheta_j)T^{ij}_{fi}, \tag{2}$$

where space $\mathbf{x}$ and time t coordinates are implicit and summation is over all j angle bands of the discretization. The transformation tensor T^{ij}_{fi} is expressed as

$$T^{ij}_{fi} = A^2[\beta|D(\vartheta_{ij})|^2\Delta\vartheta + \delta(\vartheta_{ij})(1 + |\alpha_c D(0)|^2) + \delta(\pi - \vartheta_{ij})|\alpha_c D(\pi)|^2], \tag{3}$$

where δ is the Dirac delta function and $\Delta\vartheta$ is the angular increment in ϑ_i and $\vartheta_{ij} = |\vartheta_i - \vartheta_j|$.

The coherent scattering coefficient, α_c in Eq. (3), depends on the distance between ice floe centers D_{av} and floe radius a, and may be expressed as

$$\alpha_c = \sqrt{\frac{2\pi}{k}}\, e^{i\pi/4} \frac{2}{\sqrt{3}D_{av}^2\sqrt{1 - 8a^2/(\sqrt{3}D_{av}^2)}} \times \int_0^\infty e^{ikx_s}\left(1 - \frac{8a^2}{\sqrt{3}D_{av}^2}\right)^{x_s/2a} dx_s, \tag{4}$$

where k is the wavenumber. The coefficient β in Eq. (3) is a cumulative expression for the *effective* density of wave scatterers, $\rho_e(r)$, defined as

$$\beta = \lim_{R\to\infty} \int_0^R \rho_e(r)dr. \tag{5}$$

If the scattering process is limited to some finite time period Δt, then Eq. (5) becomes

$$\beta = \int_0^{R_{\max}} \rho_e(r)dr, \tag{6}$$

where $R_{\max}$ is the *maximum* distance traveled by waves during time period Δt. The *effective* density of ice floe scatterers, $\rho_e(r)$, radiating waves to position $\vec{r}$, is

$$\rho_e(r) = \frac{\text{fi}}{\pi a^2\sqrt{1 - (4\text{fi}/\pi)}}\left(1 - \frac{4\text{fi}}{\pi}\right)^{r/2a}, \tag{7}$$

where fi represents ice cover concentration. This follows from having the single scattering approximation and an assumed infinite hexagonal lattice of ice floes.

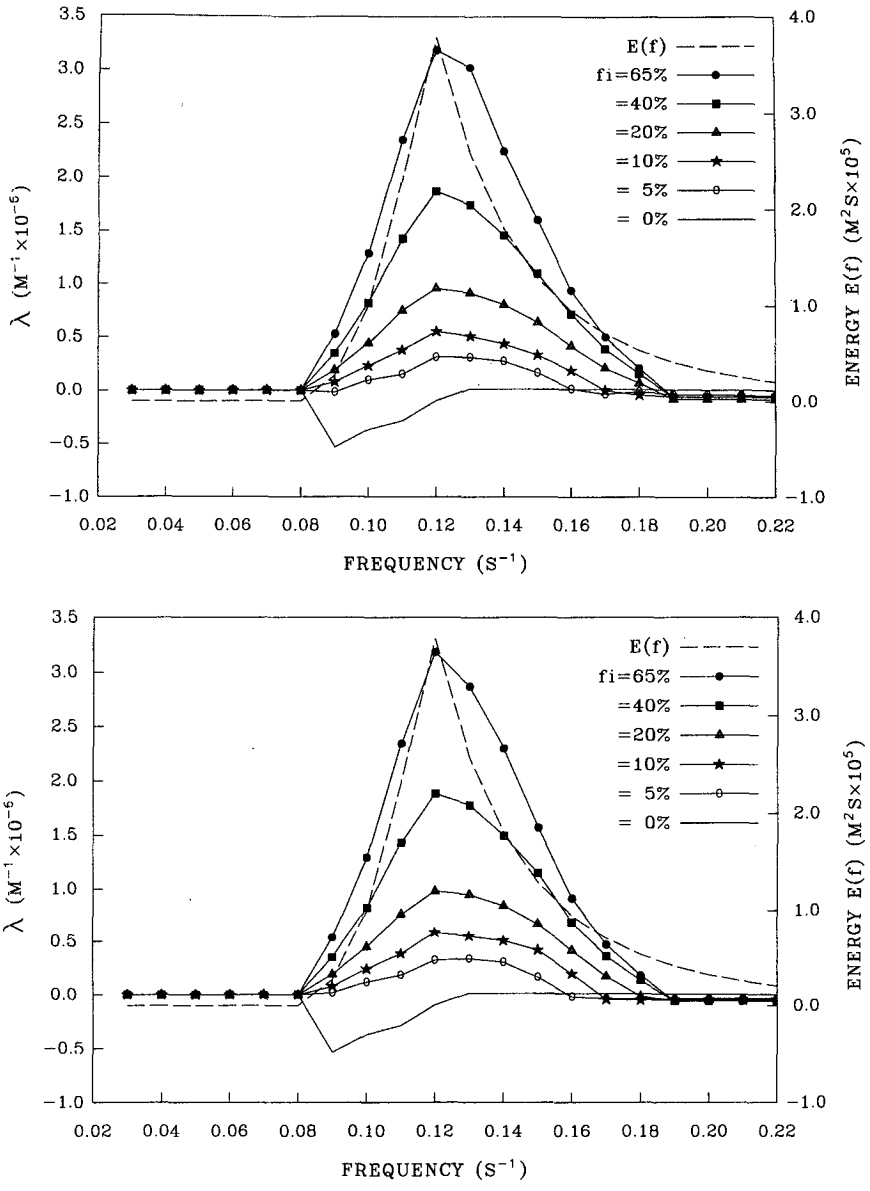

FIG. 3. Wave attenuation λ as a function of frequency f and ice cover concentration fi. The energy impinging on the MIZ is given by $E(f)$ assuming (a) 20-m floe diameter and 1.5-m floe thickness, (b) 20-m floe diameter and 3.0-m floe thickness and (c) 15-m floe diameter and 1.5-m thickness.

The coefficient A, in Eq. (3), is necessary for normalization of the scattered energy. It is defined as

$$A = (1 + |\alpha_c D(0)|^2 + |\alpha_c D(\pi)|^2 + \beta \int_0^{2\pi} |D(\vartheta)|^2 d\vartheta + f_d)^{-1/2}, \quad (8)$$

where f_d is expressed in terms of the absorption cross section, σ_a, as

$$f_d = (e^{\rho_0 \sigma_a C_g \Delta t} - 1), \quad (9)$$

and $\rho_0 = 2/(\sqrt{3}D_{av}^2)$, as derived by Masson and LeBlond (1989), for a regular ice floe array.

Finally, the cross-section scattering coefficient $D(\vartheta_{ij})$, in Eqs. (3) and (8), is given in terms of heave, $D_1(\vartheta_{ij})$, surge, $D_2(\vartheta_{ij})$, pitch, $D_3(\vartheta_{ij})$, and diffraction, $D_4(\vartheta_{ij})$, as

$$D(\vartheta_{ij}) = D_1(\vartheta_{ij}) + D_2(\vartheta_{ij}) + D_3(\vartheta_{ij}) + D_4(\vartheta_{ij}). \quad (10)$$

Heave $D_1(\vartheta_{ij})$, surge $D_2(\vartheta_{ij})$, and pitch $D_3(\vartheta_{ij})$ are given by

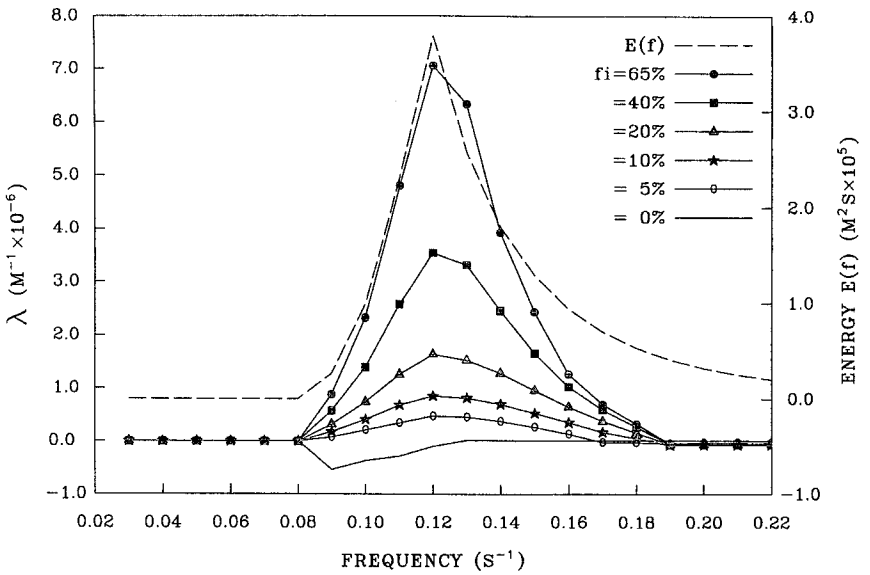

FIG. 3. (*Continued*)

$$D_b(\vartheta_{ij}) = -\frac{\omega}{g}\frac{\xi_b}{(H/2)}\sqrt{\frac{2\pi}{k}}\,C_0\cosh(kh)e^{-i\pi/4} \times \sum_{j=1}^{N}\sum_{l=0}^{\infty} f_{bl}(s_j)\cosh[k(Z_j+h)] \times J_l(kR_j)e^{-i\pi l/2}R_jL_j\cos(l\vartheta_{ij}), \quad (11)$$

where ω is angular frequency, g is the acceleration due to gravity, $H/2$ is the wave amplitude, h the water depth, and J_l is the Bessel function of the first kind of order l. Diffraction, $D_4(\vartheta_{ij})$, is similar to Eq. (11). Specification of the body motion amplitudes ξ_b, source strength distribution functions f_{bl}, and the geometrical elements R_j, Z_j, L_j, s_j, and C_0 is given in the appendix. The corresponding response amplitude operators (RAO) for the ice floe components are heave $\xi_1/(H/2)$, surge $\xi_2/(H/2)$, and pitch $L\xi_3/180H$.

Figure 1 presents the variation in heave, surge, and pitch RAOs, as a function of dimensionless wavenumber ka (the ratio of ice floe radius to wavelength). Ice floe thickness is assumed 3 m in water 30 m deep. Figure 1 verifies that our model for the ice transformation tensor T_{ij}, as introduced in Eq. (2), is approximately the same as the T_{ij} model described by Masson and LeBlond (1989) and Isaacson (1982). In the limit as $k \to 0$, corresponding to very long waves, heave and pitch asymptote to unity, whereas surge diverges. At $ka = 1$, heave has a maximum of ≈ 1.25, whereas at $ka = 1.75$, pitch has a maximum of ≈ 1.9.

3. Attenuation characteristics

Attenuation λ is understood in terms of the decay rate of the spectral wave energy, as waves propagate from the open ocean into the MIZ. To present the basic λ characteristics of the *scattering* model, we implemented the model on the simple square box SWAMP ocean, used by Hasselmann et al. (1985) in intercomparing wave models. The SWAMP ocean and wind orientation are shown in Fig. 2. Ice floes are assumed in rows of grid points parallel to the wind direction, as indicated. Attenuation λ is defined following Wadhams et al. (1988),

$$\lambda = \frac{1}{E(f,\vartheta)}\frac{\partial E(f,\vartheta)}{\partial x}, \quad (12)$$

where $E(f, \vartheta)$ is the spectral wave energy and x, the distance propagated into the MIZ from the open ocean. In this section, we derive estimates for λ as a function of (i) wave frequency, (ii) ice cover concentration, (iii) ice floe diameter, (iv) floe thickness, (v) distance measured from the ice edge x, (vi) wind speed U_{10}, and (vii) wave age. Of course, there are other variables such as ice type and ice floe shape, which were not considered in the *scattering* model, although present in real observations.

a. *Ice floe parameters*

Figure 3a presents λ as a function of frequency and ice cover concentration fi, where fi = 0%, 5%, 10%, 20%, 40%, 65%. Although observed ice cover concentration fi may be 90%, Eq. (7), giving the effective ice floe number density is not valid for ice cover concentration in excess of $\pi/4$. Figure 3a implies that as fi increases, the wave attenuation increases, approximately in proportion to fi. The associated one-dimensional wave spectrum $E(f)$ is indicated. When ice is absent (fi = 0), then λ is negative and waves are

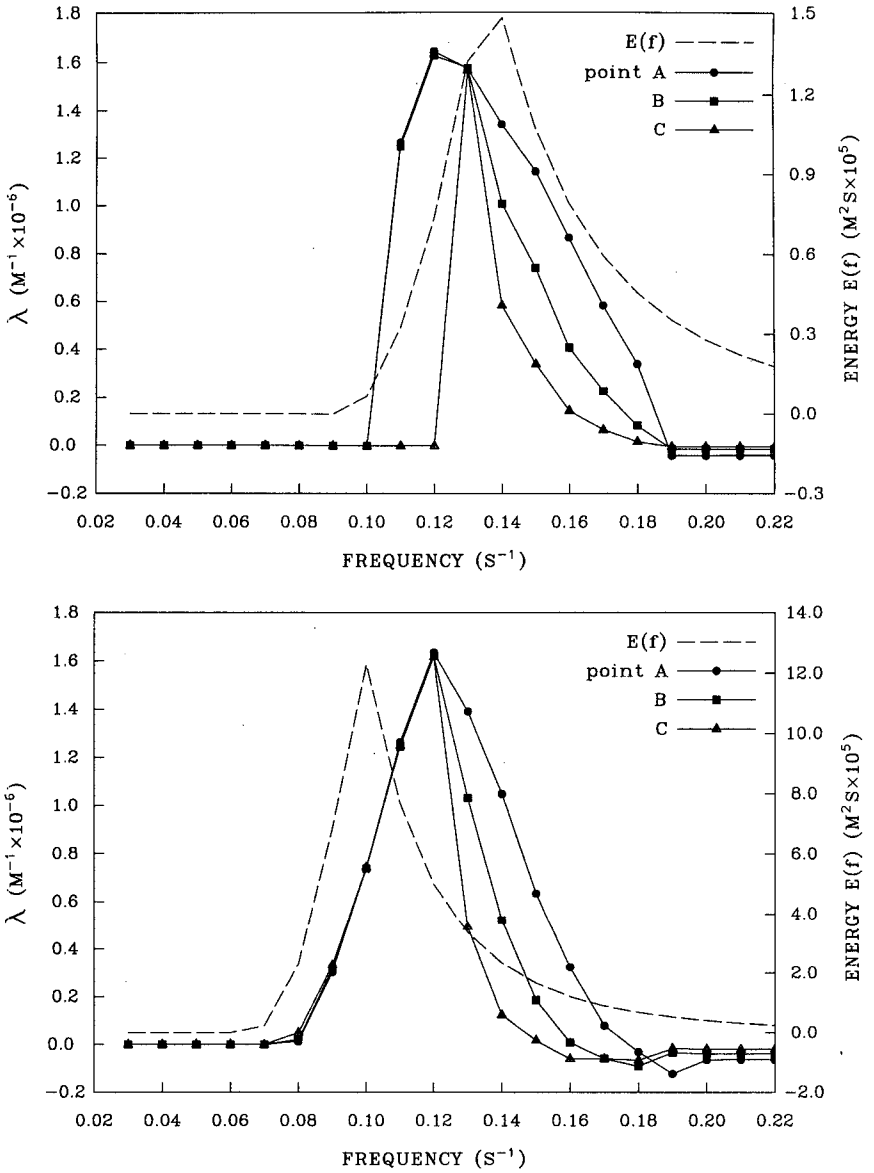

FIG. 4. Wave attenuation λ as in Fig. 3c for the 2nd, 3rd and 4th grid points within the ice edge, labeled A, B, and C in Fig. 2. These points are at 20, 30, and 40 km from the ice edge. Energy $E(f)$ impinging on the MIZ is indicated assuming a wind speed (a) U_{10} = 15 m s^{-1} and (b) U_{10} = 30 m s^{-1}.

generated and grow. In obtaining these results, we have assumed the wind speed U_{10} is 20 m s^{-1}. Space discretization Δx is 10 km and the time step Δt is 300 sec. The ice floes are assumed to have diameter 20 m and thickness 1.5 m. In order to allow the model to approximately reach equilibrium, λ is reported after the model has simulated 20 h. Unless otherwise noted, the centered difference scheme was used in solving Eq. (12) for λ at the second grid point within the MIZ.

To demonstrate the effect of floe thickness, we present λ for ice floes 3 m thick, in Fig. 3b. The difference in λ is less than 5% between Figs. 3a and 3b, whereas the floe thickness differs by 2 times. All other conditions are the same. The effect of ice floe diameter d is given in Fig. 3c. This repeats Fig. 3a except that floe diameters are 15 m rather than 20 m. The variation of λ in Fig. 3c is similar to that of Figs. 3a,b except the scale is approximately doubled. Thus, floe diameter d appears to be a more important factor in λ than floe thickness.

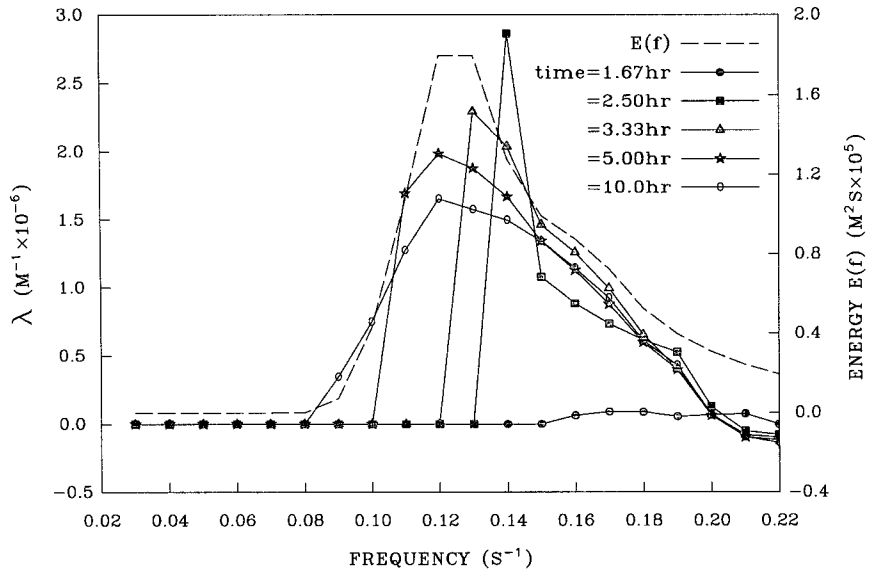

FIG. 5. Wave attenuation λ as in Fig. 3c as a function of time $t = 12/3, \cdots, 10$ h. Corresponding wave ages are 0.23, 0.25, 0.27, 0.30, and 0.40, respectively. There were no waves at $t = 0$. Energy $E(f)$ at $t = 10$ h is indicated. Assumed wind speed is 20 m s^{-1}. Floes are 1.5 m thick and 15 m in diameter and fi = 20%.

b. Wind, position, and wave age

Given waves that propagate from open ocean into the MIZ, λ may depend on wind speed U_{10} and the distance from the ice edge. To investigate this, we present λ as a function of U_{10} and MIZ position in Figs. 4a,b. Results are shown for 15 and 30 m s^{-1} winds, using the second, third, and fourth grid points within the MIZ, denoted A, B, and C in Fig. 2. Figures 4a,b are similar, despite the fact that U_{10} is 2 times larger in Fig. 4b than in Fig. 4a. Differences in λ are apparent in the high-frequency portion of the spectrum as a function of MIZ position. However, energy in low-frequency bands is not strongly attenuated. This is particularly evident in Fig. 4b, where higher wind speeds are associated with much higher wave energy $E(f)$ and a lower spectral peak f_p. Therefore, although $E(f)$ is highly dependent on U_{10} and MIZ position, λ is largely independent of these factors.

As waves are generated and evolve, the balance of spectral wave energy differs from the equilibrated (or saturated) state. In the equilibrium state presented in Figs. 3–4, the advection of energy $\vec{C}_g \cdot \nabla E(f, \vartheta)$, energy input by the wind S_{in}, and energy transferred from other parts of the spectrum S_{nl} establish a balance with energy lost through dissipation S_{ds}. This balance is not possible when waves are growing, as the spectral peak f_p rapidly decreases. Because λ is highly dependent on frequency f, we expect λ should also depend on wave growth and spectral maturity. Specifically, we expect λ should depend on wave age $g/(2\pi f_p U_{10})$ as a measure of wave maturity. Figure 5 presents λ as a function of wave age for the same conditions as Fig. 3c. As time evolves, the peak in λ shifts to lower frequency f. Moreover, the scale of λ varies as the seastate evolves. Peak λ values decrease as waves get older. The transition occurs quickly. Within 5 h of simulated time, estimates for λ are close to the "long time" asymptotic values reported in Figs. 3–4.

4. Impact of scattering and attenuation on the wave spectrum

Except for Wadhams et al. (1986), there is little data to validate an investigation of the impact of wave attenuation λ on the wave spectrum. Obviously it is difficult to mount a large-scale experiment involving the mooring of directional buoys in the MIZ. Within a few hours, the ice distribution may change and the instruments could be lost. The tests described in this section consider the scattering model, implemented on the SWAMP ocean of Fig. 2 with an assumed array of ice floes. Wave energy is estimated as a function of (i) ice cover concentration fi, (ii) ice edge geometry, (iii) a single ice floe diameter d assumed uniformly for the whole MIZ, and (iv) variable MIZ ice floe diameters. This is motivated by section 3, which showed that fi and d are important factors in controlling λ.

a. Ice cover concentration

Typically, ice cover concentration fi may be expected to increase gradually in proceeding from open ocean, through the MIZ and into pack ice. Thus, we

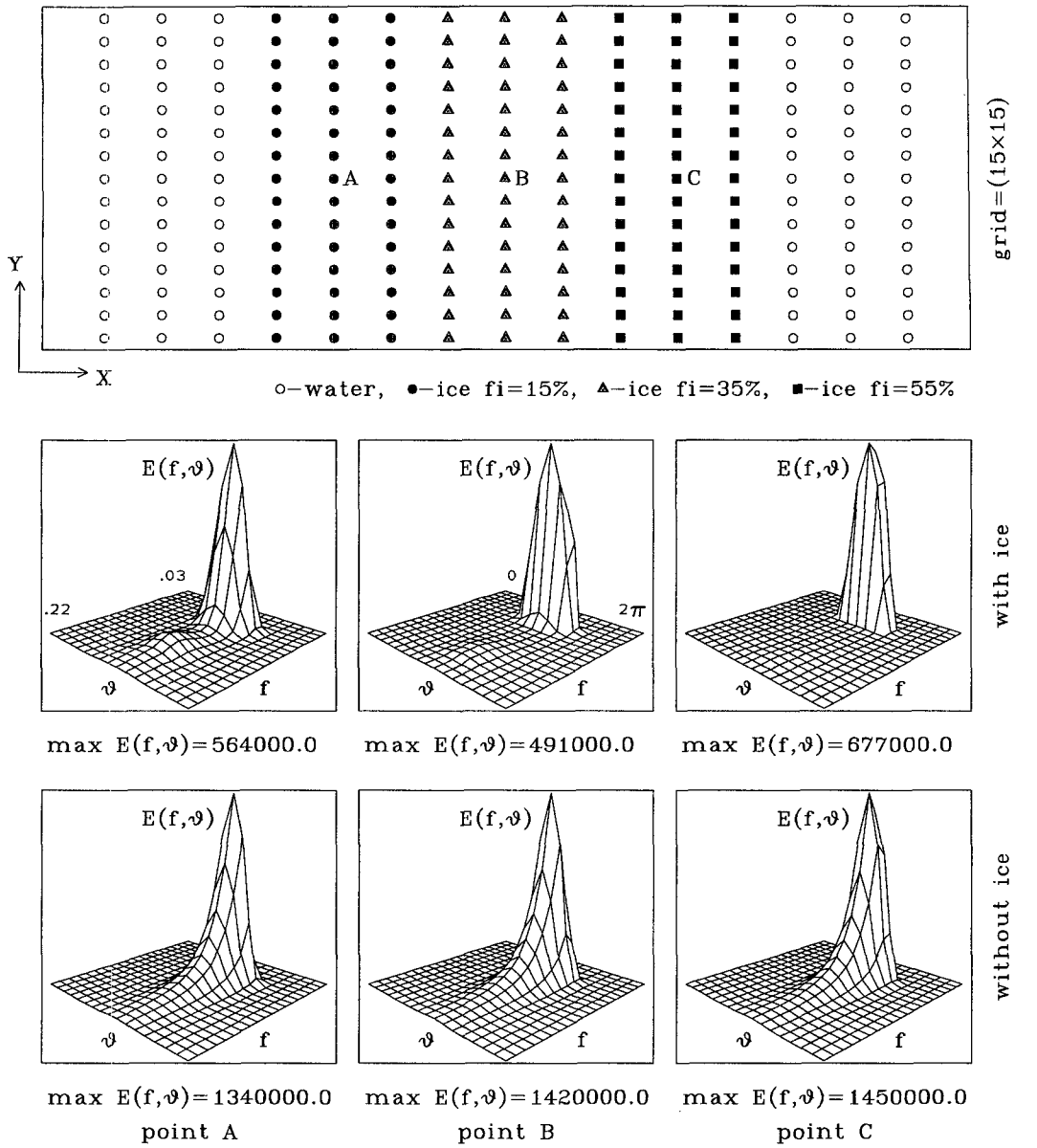

FIG. 6a. The two-dimensional wave spectra $E(f, \vartheta)$, are presented at positions A, B, and C within the MIZ ice floe array, denoted "with ice" and "without ice." Floe diameter is 10 m and wind speed is 20 m s^{-1}. The grid consists of water points, indicated by the symbol O. Ice points, with fi = 15%, 35% and 55%, are indicated by solid symbols in the figure. Gridpoint separations in both the X and Y directions is 100 km, uniformly. The fetch for A, B, and C is X = 500, 800, and 1100 km. To set the energy scale, the maximum for $E(f, \vartheta)$ is given in each plot. The frequency f varies from 0.03 to 0.22 Hz, and direction ϑ varies from 0° to 360° as indicated.

consider ice cover concentrations fi of 15%, 35%, and 55% at positions A, B, and C within the ice floe array, as indicated in Fig. 6a. The resultant two-dimensional energy $E(f, \vartheta)$ shows a reduction of high-frequency wave energy with fetch X, in moving from A to B and its virtual dissipation at C. Essentially, the wave spectrum is reduced to a low-frequency rump at C compared to the more rounded $E(f, \vartheta)$ at A just inside the MIZ. Corresponding plots of $E(f, \vartheta)$ for open ocean "without ice" conditions are also given. The assumed wind speed U_{10} is 20 m s^{-1}, the ice floe diameter is 10 m and the ice thickness is 1.5 m. The grid spacing is 100 km, implying that A, B, and C are at fetch X = 500, 800, and 1100 km, respectively. Results in Fig. 6a are reported after the *scattering* model has simulated 20 h. Prior to time t = 0, several days of real time were sim-

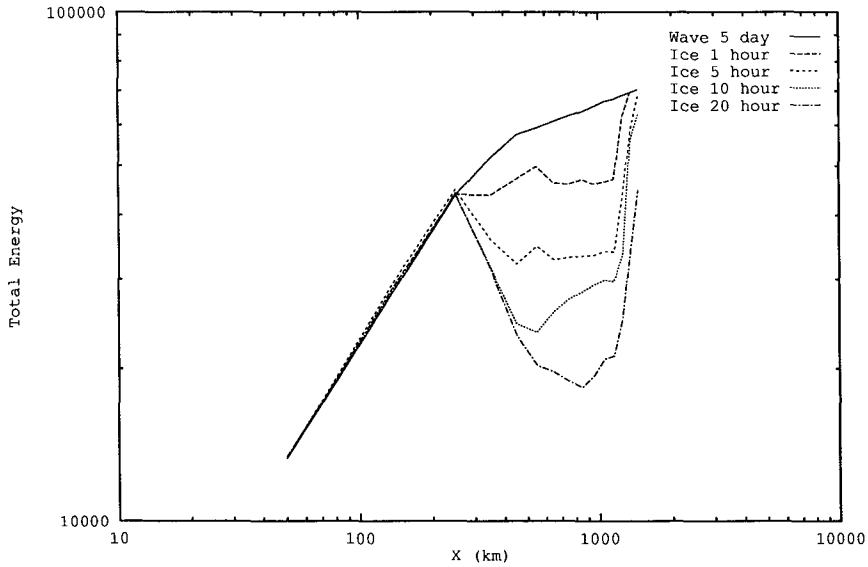

FIG. 6b. The fetch-growth relations for total energy E_0 and fetch X corresponding to Fig. 6a.

ulated with the wave component of the scattering model to allow "spin up" time for the waves.

The so-called fetch-growth curves, relating total energy E_0 to fetch X, where

$$E_0 = \int_0^{\infty} \int_0^{2\pi} E(f, \vartheta) df d\vartheta \qquad (13)$$

are presented in Fig. 6b. Fetch-growth curves are usually presented in field experiments, such as JONSWAP by Hasselmann et al. (1973), and numerical studies such as the SWAMP study of Hasselmann et al. (1985). Figure 6b shows that total energy E_0 is quickly damped after time $t > 0$ h. After only 1 h, E_0 is reduced by $\approx$25%. After 5 h, the reduction is $\approx$50%. Of course, at fetch $X \geq 1300$ km, which is beyond the ice array, the spectrum grows rapidly.

b. Ice edge geometry

MIZ observations must describe the ice edge geometry carefully. In Figs. 6a,b we considered columns of ice floes extending across the SWAMP ocean. Had we considered a simple localized array of ice floes as depicted in Fig. 7, results would be different. The directional distribution of wave energy $E(f, \vartheta)$ allows the propagation of energy in directions that are nonparallel to the wind, entering the MIZ from the *sides* in Fig. 7. In place of the simple sharp peak shown in Fig. 6a, a broad peak results, propagating largely in the wind direction. If the integration is continued for several days, the $E(f, \vartheta)$ peak splits into two peaks at directions differing slightly from the wind direction: $\sim \pm 45°$, or two angle bands, as shown in Fig. 7, after 120 h. The attenuation of total energy E_0 is slightly less severe than was obtained in Fig. 6b, because energy propagates into the ice floe array from the array sides. Overall, the effects described here increase as the ice bands become narrower. In contrast, the ice floe columns in Figs. 6a,b do not allow this energy leakage because they extend completely across the SWAMP ocean.

c. Ice floe diameter

Figures 3a,c show that a slight change in ice floe diameter d could result in important modifications to λ. The role of d in MIZ wave spectra is explored in Figs. 8a,b. The ice cover concentration fi is assumed 15% throughout the array. When $d = 15$ m, as in Fig. 8a, wave spectra $E(f, \vartheta)$ are similar to those of Fig. 6a. However, in Fig. 8a, $E(f, \vartheta)$ has nontrivial energy in middle and high frequency portions at positions B and C. Corresponding energy is dissipated in Fig. 6a. In Fig. 8a, wave energy can grow within the MIZ. Figure 8b, where $d = 6$ m, shows that decreasing d results in enhanced λ and reduced $E(f, \vartheta)$ compared to Fig. 8a, particularly in middle and high frequency spectral regions. These results are consistent with Figs. 3a,c.

d. Multiple ice floe diameters

In general, ice is observed to act as a low-pass filter. Only the low-frequency swell penetrates to great distances within the pack ice. This occurs because all the middle and high frequency wave energy is dampened by a myriad of MIZ ice floe sizes. Floes range from kilometer-scale diameters down to centimeter-scale diameters and occur in all shapes. However, if only a specific diameter such as 20 m is present, we expect

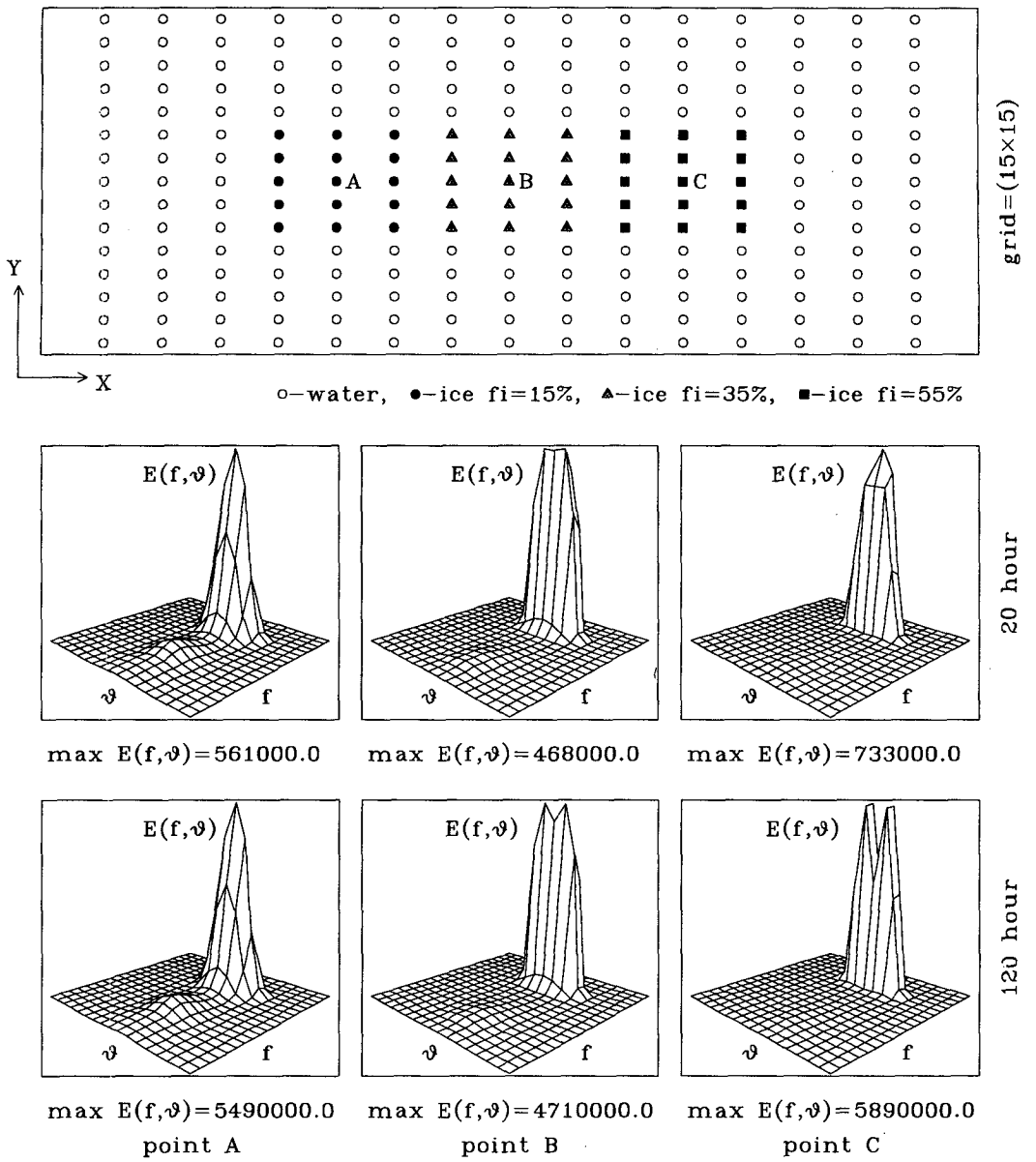

FIG. 7. The variation of $E(f, \vartheta)$ with position and time, assuming the concentrations fi and floe diameter d of Fig. 6a, arranged in a localized array of ice floes.

that only specific regions of the spectrum should be dampened, involving a resonant frequency and harmonics. This is suggested analytically by Perrie and Rahman (1991) for fixed cylinder floes.

Ice floes typically vary in size, with the smallest ice floes at the ice edge, where waves have broken up larger ice floes. Larger ice floes are usually within the MIZ, at some distance from the ice edge. To investigate the effect this may have on λ, Fig. 9a considers a 15% constant ice cover concentration fi, with floe diameters d = 10, 20, and 30 m at positions A, B, and C, respectively. Figure 9b gives the corresponding fetch-growth curves. Figures 10a,b repeat Figs. 9a,b, with the distribution of ice floes reversed: the largest ice floes are at the ice edge nearest the open ocean, where waves are being generated, and the smallest floes are at an ice edge within the MIZ. In Figs. 9a,b, it is evident that energy is attenuated at B relative to A and then begins to show significant growth at C. Increasing the floe diameter at C relative to B and A, results in growth in wave energy $E(f, \vartheta)$ in low, middle, and high regions of the spectrum at C, as suggested by Figs. 8a,b. In contrast to this, the fetch-growth curves in Fig. 10b are somewhat inverted relative to Fig. 9b: total energy E_0

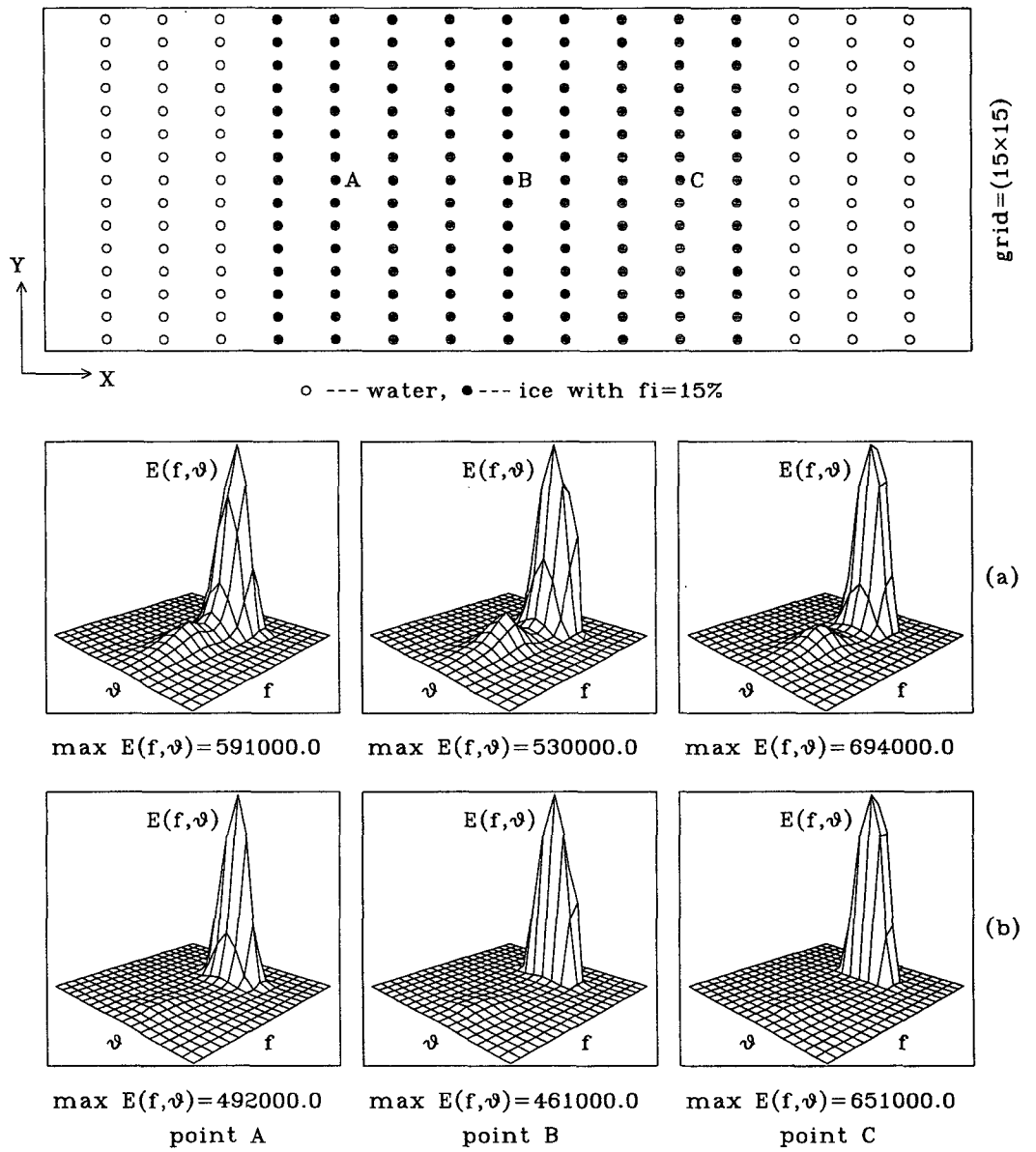

FIG. 8. The variation of $E(f, \vartheta)$ with position, as in Fig. 6a, with fi = 15% and assuming floe diameter (a) d = 15 m and (b) d = 6 m.

decreases with fetch X and with reduction in floe diameter. Reducing the floe diameter results in significant reduction in middle and high frequency spectral energy $E(f, \vartheta)$ and only slight growth in low-frequency spectral energy (at C relative to B and A in Fig. 10a).

5. Wave attenuation observations

The difficulty in comparing model estimates for wave attenuation with MIZ observations, is that ice concentration fi, and ice floe diameter and thickness are well known and measured in only localized neighborhoods, where intensive field experiments have been conducted. On the scale of hundreds or thousands of kilometers, these measurements are not generally available. Typical ice charts for the Labrador Sea and Newfoundland shelf give overall ice field characteristics down to the scale of about 50 km. However, ice parameters may still vary considerably over the 10–100-km grid size typical of wave model implementations for the North Atlantic. Moreover, the models make several assumptions. The scattering model assumes cylindrical ice floes of uniform thickness located in a regular spatial array that remains fixed in time. In reality, ice floes

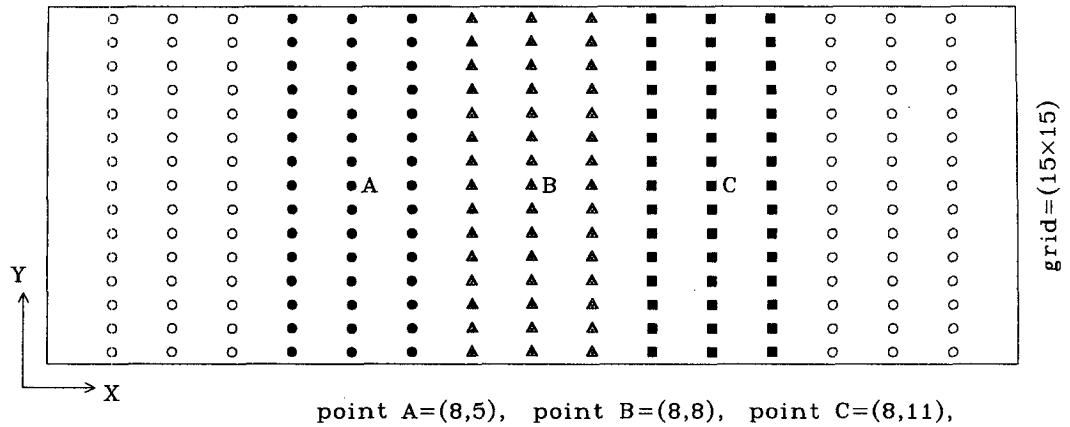

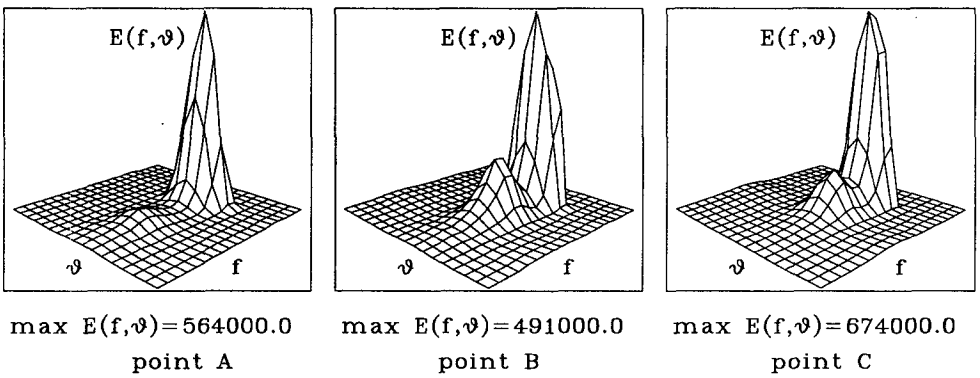

FIG. 9a. As in Fig. 6a, the variation in $E(f, \vartheta)$ with position A, B, and C within the MIZ, assuming a constant fi of 15% and floe diameters d of 10 m at A, 20 m at B, and 30 m at C.

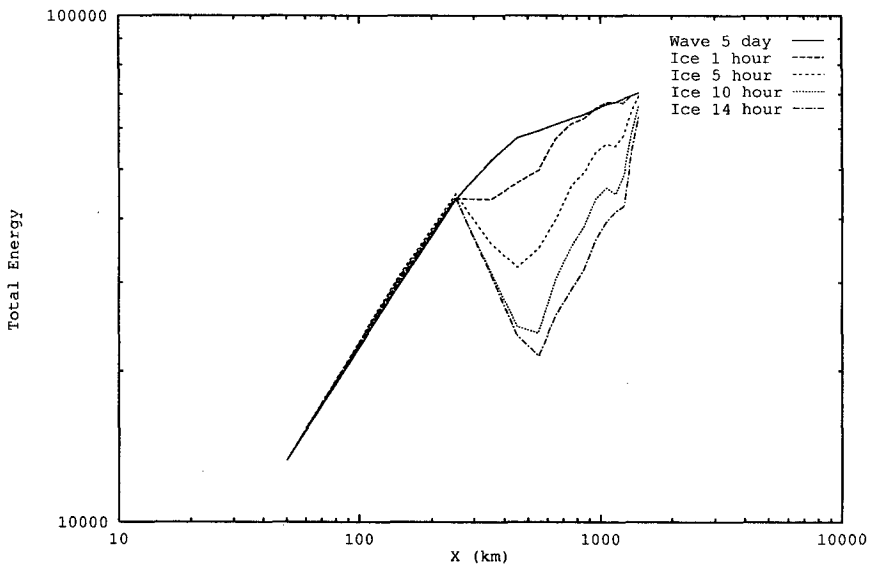

FIG. 9b. The fetch-growth relations for E_0 and X for Fig. 9a.

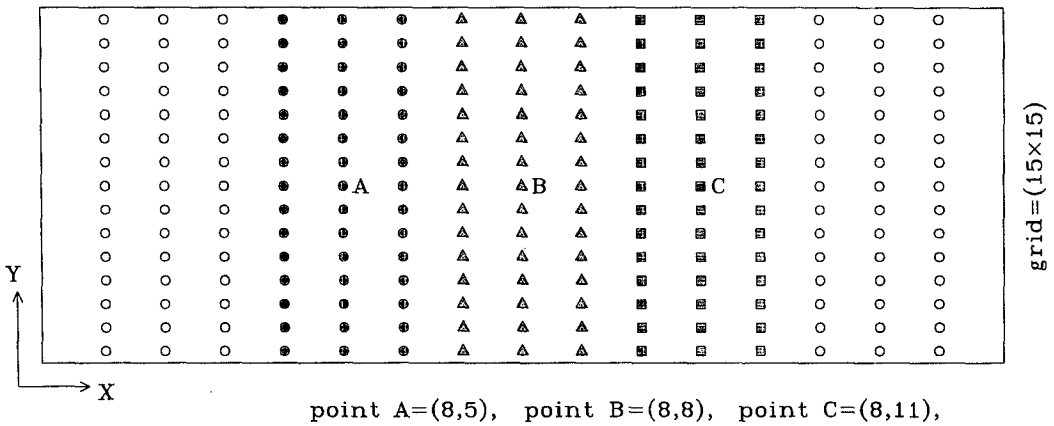

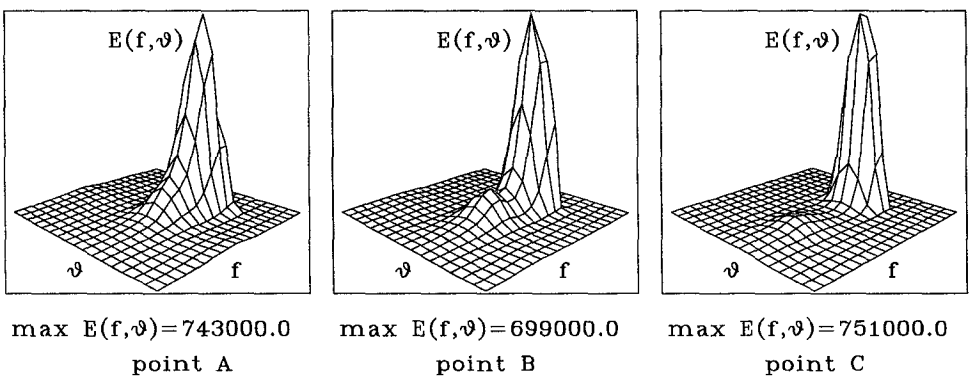

FIG. 10a. As in Fig. 9a, the variation in $E(f, \vartheta)$ with position A, B, and C, assuming floe diameters d = 30 m at A, 20 m at B, and 10 m at C.

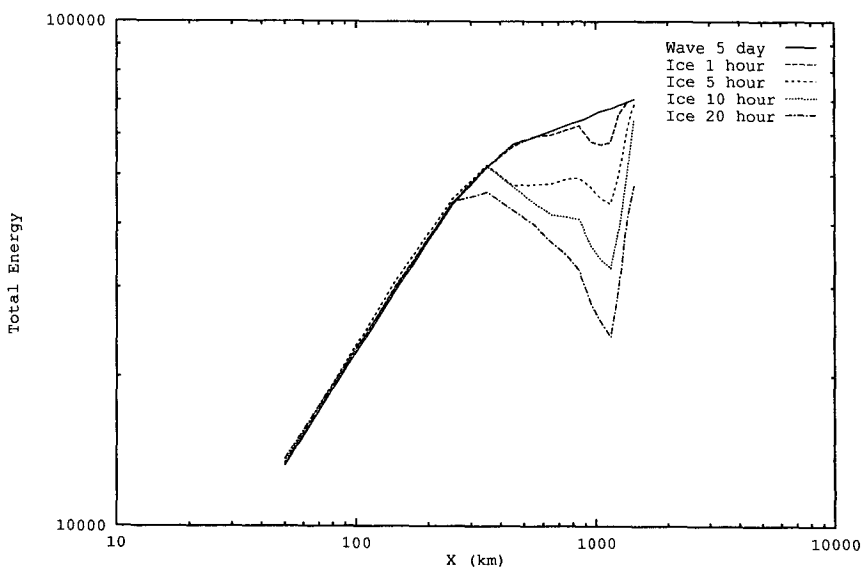

FIG. 10b. The fetch-growth relations for E_0 and X for Fig. 10a.

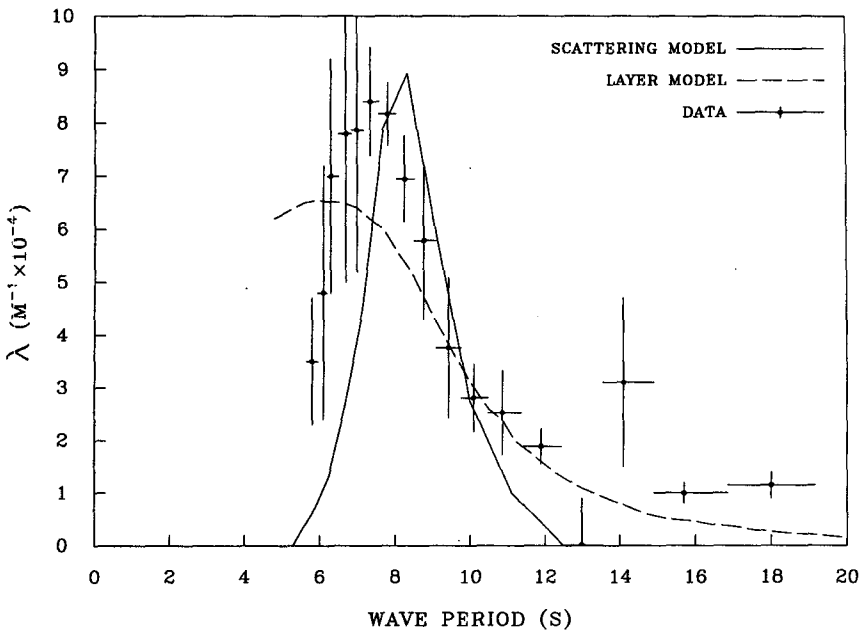

FIG. 11a. Comparison of λ estimates from the scattering model, the layer model and MIZEX data from the Bering Sea on 7 February 1983.

are irregularly shaped, with variable thickness, irregular positions, and they drift in response to atmosphere–ocean forcing.

Liu et al. (1991) present measurements of wave attenuation λ, as collected by Wadhams et al. (1988) during MIZEX, in comparison with their model estimates. Their model, as described by Liu and Mollo-Christensen (1988), is hereafter referred to as a *layer* model. Examples of the measurements are given in Fig. 11a. In comparing the scattering model with data, we

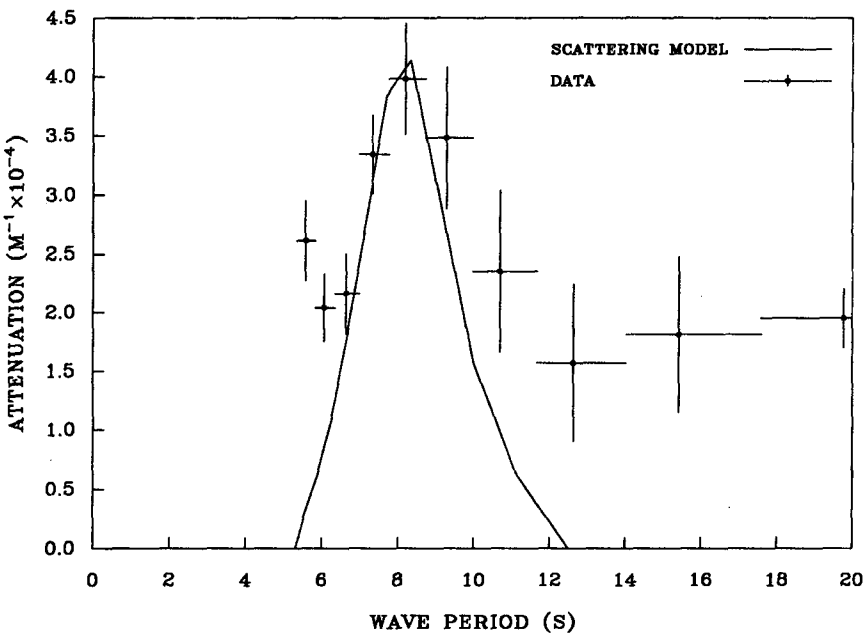

FIG. 11b. Comparison of λ estimates from the scattering model and MIZEX data from the Greenland Sea on 18 September 1978.

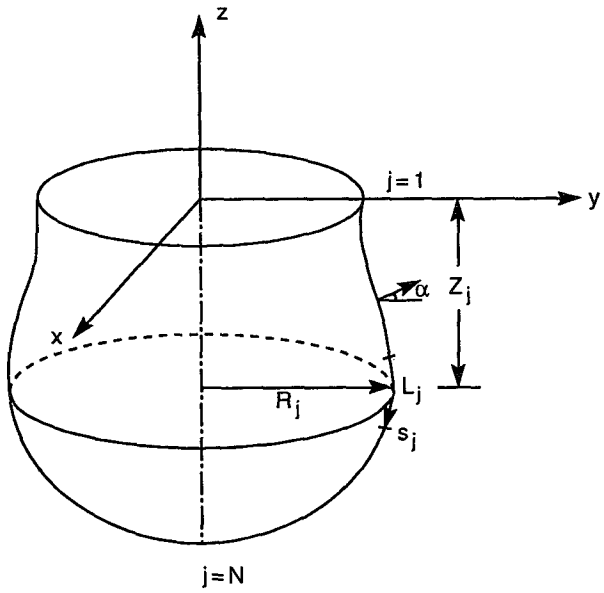

FIG. 12. Geometry of symmetrical ice floes. The summation in equations (11) and (15) goes from $j = 1$ to $j = N$, as indicated. Integration variables, corresponding to the jth integration element s_j, are R_j, Z_j, and L_j. The angle from normal, α in Eq. (21) for g_{4l}, is shown.

have assumed the floe diameter d is 14.5 m, U_{10} is 20 m s^{-1}, and floe thickness 1.5 m. A comparison of the layer and scattering models is shown in Fig. 11a. In the limit as wave period approaches zero, the scattering model tends to be more able to match the reductions in λ reported in observations than the layer model. As shown in Fig. 11a, the layer model asymptotes to a plateau as the wave period approaches zero. Moreover, the scattering model λ tends to match the maximum observed λ. A further comparison of scattering model estimates with MIZEX measurements is given in Fig. 11b. Model estimates are again shown to match the measured peak λ values. A 10% ice cover concentration with 8-m diameter floes was assumed in Fig. 11b.

6. Conclusions

We have considered the relation between wave attenuation λ, MIZ ice floe parameters, wind, and wave conditions. Using the scattering model, we have shown that:

(i) Wave attenuation λ depends strongly on wave frequency f, floe diameter d, ice cover concentration fi, and wave age.

(ii) Ice floe thickness, wind speed U_{10}, wave energy $E(f, \vartheta)$, and spatial position within the MIZ were shown to be less important factors.

(iii) Under appropriate MIZ conditions (regarding fi and d), generation and wave growth occurs. Under other conditions, all energy but that of the very lowest-frequency bands is dissipated.

For example, as fi increases or as d decreases, we have shown that λ increases dramatically, with a strong dependence on wave frequency f.

Wave attenuation λ estimates from the scattering and layer models were compared with MIZEX data. While the scattering model is comparable to the layer model in being largely able to estimate λ, it appears to be slightly better at modeling λ for low-frequency spectra. Both models are limited by their assumptions, as noted earlier. The layer model assumes a value for the eddy viscosity. The scattering model assumes an ice cover concentration fi, an ice floe diameter d, a single scattering approximation and floes positioned in regular lattice arrays. Part II of this study considers ice floe drift experienced in response to waves, wind, and currents, integrated with MIZ wave attenuation and scattering.

A comprehensive field effort is needed to quantitatively measure the geometry of the MIZ ice floes, the ice floe array distribution, the wave spectrum and its evolution during storm situations, before a full understanding of MIZ wave dynamics is possible. Although Wadhams et al. (1986) attempted to measure the wave spectra inside the MIZ, they were hindered by limited data regarding ice conditions, such as floe size and thickness distributions. However, they did make conclusions that are largely in agreement with our results. They found that MIZ pack ice attenuates waves differentially: short waves are dampened more than long waves. They suggested that wave generation may occur in low ice cover concentration fi situations. They also suggested that wave spectra should become isotropic soon after entering the MIZ and that swell spectra required a longer distance, but ultimately also becomes isotropic.

Acknowledgments. The wave modeling program at BIO is funded by the Federal Panel on Energy Research and Development (Canada) under Project 6B3006. The authors want to express their thanks to Erik Mollo-Christensen and a reviewer for numerous important comments on our manuscript and for patience in reading the original manuscript.

APPENDIX

Body Motion Amplitudes

The body motion amplitudes ξ_b may be specified as the solutions to the Fourier transformed linearized equations of motions for a floating axisymmetric ice floe

$$\sum_{b=1}^{3} [-\omega^2(m_{ib} + a_{ib}) - i\omega b_{ib} + c_{ib}]\xi_b = \mathcal{F}_i^e, \quad \text{(A1)}$$

where $i = 1, 2, 3$; m_{ib} is the mass matrix, c_{ib} the hydrostatic stiffness coefficient, $\mathcal{F}_i^e$ the exciting forces associated with incident and diffracted wave potentials ($\phi_0 + \phi_4$), a_{ib} the added mass coefficients for a given ice

floe, and b_{ib} the damping coefficients. The corresponding source strength distribution functions $f_{bl}(s_j)$, in Eq. (11), have to be computed for each particular floe shape used in the model. Assuming symmetrical ice floes, as shown in Fig. 12, the functions f_{bl} are defined by the relation

$$\sum_{j=1}^{N} A_{ij}^{l} f_{bl}(s_j) = B_i^{bl}, \tag{A2}$$

where the extent of the summation, $j = 1, N$, is indicated. The jth integration element s_j of the summation in Eq. (A2) extends from the top surface ($j = 1$) to the midpoint of the jth incremental element L_j, as indicated. Functions A_{ij}^{l} and B_i^{bl} are given by

$$A_{ij}^{l} = \int_{L_j} R_j \sum_{m=0}^{\infty} \frac{\partial G_{lm}}{\partial n}(s_i, s')ds' - \delta_{ij}, \tag{A3}$$

$$B_i^{bl} = 2g_{bl}(s_i) \tag{A4}$$

for $i = 1, 2, \cdots, N$; $l = 0, 1, \cdots$; $b = 1, 2, 3, 4$. Radial coordinate R_j is indicated in Fig. 12. As may be inferred from Isaacson (1982), g_{bl} may be expressed in terms of J_l, the Bessel function of the first kind of order l,

$$g_{11} = -i\omega \cos\alpha \tag{A5}$$

$$g_{20} = -i\omega \sin\alpha \tag{A6}$$

$$g_{31} = -i\omega(z \cos\alpha - r \sin\alpha) \tag{A7}$$

$$g_{4l} = \frac{igkH}{2\omega} \frac{\beta_l}{\cosh(kh)} \{\sinh[k(z + h)] \sin\alpha J_l(kr) + \cosh[k(z + h)] \cos\alpha J_l'(kr)\} \tag{A8}$$

for all l, where $\beta_0 = 1$, and $\beta_l = 2i^l$ when $l \geq 1$. Otherwise, $g_{bl} = 0$. Angle α is relative to normal, as indicated in Fig. 12. From Isaacson (1982), the Green's function $G_{lm}(s_j, s')$ may be expressed as

$$G_{lm}(s_j, s') = 4C_m \cos[\mu_m(Z_j + h)] \times \cos[\mu_m(z + h)] K_l\begin{pmatrix}\mu_m r \\ \mu_m R_j\end{pmatrix} I_l\begin{pmatrix}\mu_m R_j \\ \mu_m r\end{pmatrix}, \tag{A9}$$

where

$$C_m = \frac{\mu_m^2 + \nu^2}{(\mu_m^2 + \nu^2)h - \nu} \tag{A10}$$

and μ_m are roots of $\mu_m h \tan(\mu_m h) = -\nu h$, where $m = 0, 1, \cdots$. Vertical coordinate Z_j is indicated in Fig. 12, in relation to R_j, L_j, and s_j.

REFERENCES

Hasselmann, K., 1962: On the nonlinear energy transfer in a gravity-wave spectrum. Part 1: General theory. *J. Fluid Mech.*, **12,** 481–500.

——, 1974: On the spectral dissipation of ocean waves due to white-capping. *Bound.-Layer Meteor.*, **6,** 107–127.

——, and Coauthors, 1973: Measurements of wind-wave growth and swell decay during the Joint North Sea Wave Project (JONSWAP). Dtsch. Hydrogr. Z., **A8**(12), 95 pp.

Hasselmann, K., and Coauthors, 1985: *Ocean Wave Modeling.* Plenum, 256 pp.

Hasselmann, S., K. Hasselmann, G. K. Komen, P. Janssen, J. A. Ewing, and V. Cardone, 1988: The WAM model—A third generation ocean wave prediction model. *J. Phys. Oceanogr.*, **18,** 1775–1810.

Isaacson, M. de St Q., 1982: Fixed and floating axisymmetric structures in waves. *J. Waterw., Port. Coastal and Ocean Div. ASCE,* **WW2,** 180–199.

Ishimaru, A., 1978: Wave propagation and scattering in random media. *Multiple Scattering, Turbulence, Rough Surfaces and Remote Sensing,* Academic Press, Vol. 2, 310 pp.

Komen, G. J., S. Hasselmann, and K. Hasselmann, 1984: On the existence of a fully developed windsea spectrum. *J. Phys. Oceanogr.*, **14,** 1271–1285.

Liu, A. K., and E. Mollo-Christensen, 1988: Wave propagation in a solid ice pack. *J. Phys. Oceanogr.*, **18,** 1702–1712.

——, B. Holt, and P. W. Vachon, 1991: Wave propagation in the marginal ice zone: Model predictions and comparisons with buoy and synthetic aperture radar data. *J. Geophys. Res.*, **96,** 4605–4621.

Masson, D., and P. LeBlond, 1989: Spectral evolution of wind-generated surface gravity waves in a dispersed ice field. *J. Fluid Mech.*, **202,** 43–81.

Perrie, W., and B. J. Toulany, 1985: Assessing a wave model á la SWAMP. Canadian Tech. Rep. of Hydro. and Ocean Sci. No. 67, 78 pp.

——, and M. Rahman, 1991: Scattering of ocean waves by arrays of cylinders with rotational symmetry. *Ocean Eng.*, **18,** 253–267.

——, H. Gunther, W. Rosenthal, and B. Toulany, 1989: Modelling wind-generated surface gravity waves using similarity in a coupled discrete wave model. *Quart. J. Roy. Meteor. Soc.*, **115,** 1373–1396.

Phillips, O. M., 1985: Spectral and statistical properties of the equilibrium range in wind-generated gravity waves. *J. Fluid Mech.*, **156,** 505–531.

Resio, D. T., 1981: The estimation of wind-wave generation in a discrete spectral model. *J. Phys. Oceanogr.*, **11,** 510–525.

Snyder, R. L., F. W. Dobson, J. A. Elliott, and R. B. Long, 1981: Array measurements of atmospheric pressure fluctuations above surface gravity waves. *J. Fluid Mech.*, **102,** 1–59.

Wadhams, P., V. A. Squire, J. A. Ewing, and R. W. Pascal, 1986: The effect of the marginal ice zone on the directional wave spectrum of the ocean. *J. Phys. Oceanogr.*, **16,** 358–376.

——, ——, D. J. Goodman, A. M. Cowan, and S. C. Moore, 1988: The attenuation rates of ocean waves in the marginal ice zone. *J. Geophys. Res.*, **93,** 6799–6818.